Multi-Angle Polarimeter Reference Spectra

Jochen Landgraf[1], Stephanie Rusli[1], Otto Hasekamp[1], Oleg Dubovik[2]

[1]SRON Netherlands Institute for Space Research, Utrecht, The Netherlands

[2] GRASP SAS, Bachy, France

Abstract:

This Technote describes the reference spectra for the Copernicus CO2M Multi-Angle Polarimeter (MAP).

1   Introduction

To formulate radiometric requirements of the MAP instrument, a set of reference spectra are simulated for a minimum, nominal and maximum radiometric scene. Additionally, spectra for an ocean glint scene and a cloudy scene for different solar zenith angles are provided. All spectra include the spectral Stokes parameter *I, Q* and *U* and the solar irradiance in the spectral range 350-1100 nm on a 1 nm spectral grid. Data are available at the ftp site of the CO_2 Spectral Sizing project ftp.sron.nl at data/ReferenceSpectra/Reference_spectra_V1.1/

2   Atmospheric Scenarios

For the simulation of MAP reference spectra, we assume a bi-module aerosol size distribution with a fine and coarse mode. Here, the log-normal size distribution of each mode is characterized by an effective radius and variance. For the fine mode, we assume purely spherical aerosol particles, whereas for the coarse mode both spherical and spheroidal aerosol particles are possible. The optical properties of spherical and spheroidal aerosol particles are calculated using the tabulated kernels of Dubovik et al. (2006).

For the simulation of the spectra, we assume the micro-physical aerosol properties to be altitude independent, whereas the number of aerosol particles for each mode is described by a Gaussian height profile with a centre height and a width parameter. Finally, to account for surface reflection we employ the BDRF kernel, which is parametrized by five kernel terms, namely

$$\boldsymbol{\rho}(\Omega_{in}, \Omega_{out}) = c_0(\lambda)\boldsymbol{K}_0(\Omega_{in}, \Omega_{out}) + c_0(\lambda)c_1\boldsymbol{K}_1(\Omega_{in}, \Omega_{out}) + c_0(\lambda)c_2\boldsymbol{K}_2(\Omega_{in}, \Omega_{out}) + c_3\boldsymbol{K}_3(\Omega_{in}, \Omega_{out}) \qquad (1)$$
$$+ c_4\boldsymbol{K}_4(\Omega_{in}, \Omega_{out})$$

Here ρ is the 4×4 surface BDRF that maps the four Stokes parameters I, Q, U and V of the incident light to the corresponding Stokes parameters of the reflected light as a function of the solid angles $\Omega_{in}, \Omega_{out}$. The BDRF kernels empirically describe the bidirectional reflection of the Earth surface, where kernel $\boldsymbol{K_i}$ with $i = 0,1,2$ simulates the radiance reflection with a wavelength dependent coefficient $c_0(\lambda)$ and two spectrally

independent coefficients c_1 and c_2. Here, the kernel K_0 models Lambertian isotropic reflection and so coefficient c_0 corresponds to the spectral Lambertian albedo. In this study, we considered a soil-type surface with Lambertian albedo of (0.13, 0.30, 0.26) at (765,1600, 2000) nm and a vegetation-type surface with Lambertian albedo of (0.44, 0.23, 0.06) at (765,1600, 2000) nm, respectively. Kernel K_1 and K_2 are adapted from the Ross-Li BDRF model describing anisotropic scalar reflection of land surfaces (A. H. Strahler et al., 1999), where K_1 simulates reflection of dense leaf canopy and K_2 the radiance reflection of a sparse ensemble of surface objects casting shadows on the background, which is assumed Lambertian. Finally, the polarizing effect of surface reflection is expressed by the kernels K_3 and K_4 representing reflection properties of vegetation and soil surfaces. Here, the polarizing effect is nearly independent of wavelength as validated with RSP aircraft measurements (Litvinov P. et al., 2012). For the radiative transfer simulation, we used the vector model V-Lintran as described by Hasekamp and Landgraf (2002, 2005a).

Overall, for the MAP performance analysis we consider three generic cases:

Case 1: Coarse and fine mode of atmospheric aerosol is located in the tropospheric boundary layer. The coarse mode has a fixed small optical depth of 0.02, the optical depth pf the fine mode varies.

Case 2: The Gaussian profile of the coarse mode is at 8 km altitude, whereas the fine mode is located in the boundary layer as for case 1. The fine mode has a fixed optical depth of 0.2, the optical depth of the coarse mode varies.

Case 3: Same as case 2 but for a 4 km layer height of the coarse mode.

For the three scenarios, the Gaussian height distribution of the coarse and fine mode are depicted in Fig. 1, the corresponding micro-physical properties are summarized in Tab. 1.
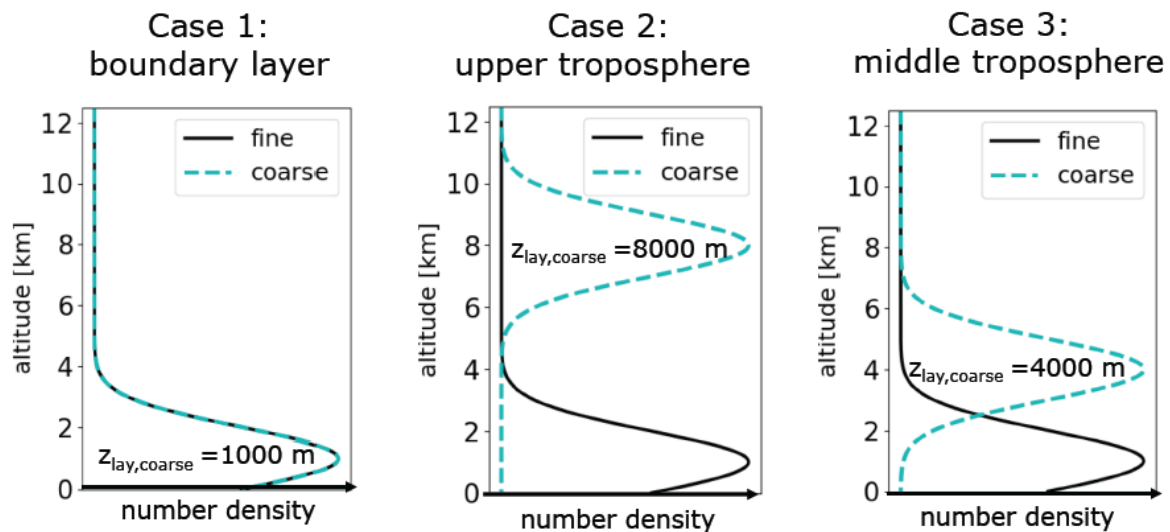
Figure 1: Aerosol profles for the coarse and file mode, The FWHM of the Gaussian profiles is 2 km in all cases..

Table 1: Micro-physical properties of the aerosol scenarios.

Aerosol parameters	Case 1		Case 2 / 3	
	Fine mode	Coarse mode	Fine mode	Coarse mode
spherical fraction	1.0	0.05	1.0	0.05
refractive index @765nm	(1.50, 1E-7i)	(1.53, 2.54E-3i)	(1.50, 1E-7i)	(1.53, 2.54E-3i)
refractive index @1600nm	(1.50, 1E-7i)	(1.40, 1.56E-3i)	(1.50, 1E-7i)	(1.40, 1.56E-3i)
refractive index @2000nm	(1.50, 1E-7i)	(1.30, 2.00E-3i)	(1.50, 1E-7i)	(1.30, 2.00E-3i)
effective radius [micron]	0.12	1.6	0.12	1.6
effective variance	0.2	0.6	0.2	0.6
z_center [m]	1000	1000	1000	8000/4000
width (FWHM) [m]	2000	2000	2000	2000

aerosol optical thickness@550 nm	varies	0.02	0.2	varies

3   Reference Spectra

To investigate the radiometric performance of different MAP instrument concepts we simulated six reference spectra:

Lmin   case 1 with total AOT=0.12, SZA=70°, VZA = 30°, soil BDRF

Lref   case 3 with total AOT=0.3, SZA=50°, VZA = 50°, vegetation BDRF

Lmax   Case 3 for total AOT = 0.3, SZA = 1°, VZA = -20°, maximum spectral radiance of a vegetation and sand spectrum including 20 % margin

Lglint   case 1 with total AOT=0.12, SZA=60°, ocean, wind speed=3 m/s

Lcld_50   Lambertian surface reflection of A=1.1 and SZA = 50°

Lcld_25   Lambertian surface reflection of A=1.1 and SZA = 25°

Lmax_alt   Case 3 for total AOT = 0.3, SZA = 1°, VZA = -20°, soil surface BDRF with 3.7 times the soil albedo term

For each spectrum, the radiance I, the relative Stokes parameters Q/I and U/I, the degree of linear polarisation (DoLP) and the solar irradiance spectra are provided for the range 350-1100 nm with a 1 nm spectral sampling. Because of its little contribution, Stokes parameter V is not reported. The spectra *Lmin*, *Lref* and *Lmax* are shown in the Figs. 2-7, including corresponding spectra for the range of viewing zenith angles between $\pm 60°$. Here Lmin comprises a relatively low radiance level with a high degree of linear polarization, whereas *Lmax* reflects a spectrum with high clear-sky radiance with a small degree of linear polarization. The figures also depict the corresponding reference values of the 3MI mission (P. Schlüssel et al.,2010) , which overall are more challenging. For Lmax this can be explained by the choice of a different reference scene, which is a cloudy scene for 3MI and a cloud-free scene in case of the MAP instrument.

Additionally, spectra are provided for a typical glint scene Lglint and for Lambertian reflection at a cloud surface with an albedo A = 1.1 and a solar angle of SZA = 25 and 50 degree, Lcld_25 and Lcld_50. For stray light analyses with a radiometric contrast within an instrument swath, we propose the use of Lmin and Lcld_25 to describe the transition between a dark scene with high DoLP and a bright scene with low (zero) DoLP.
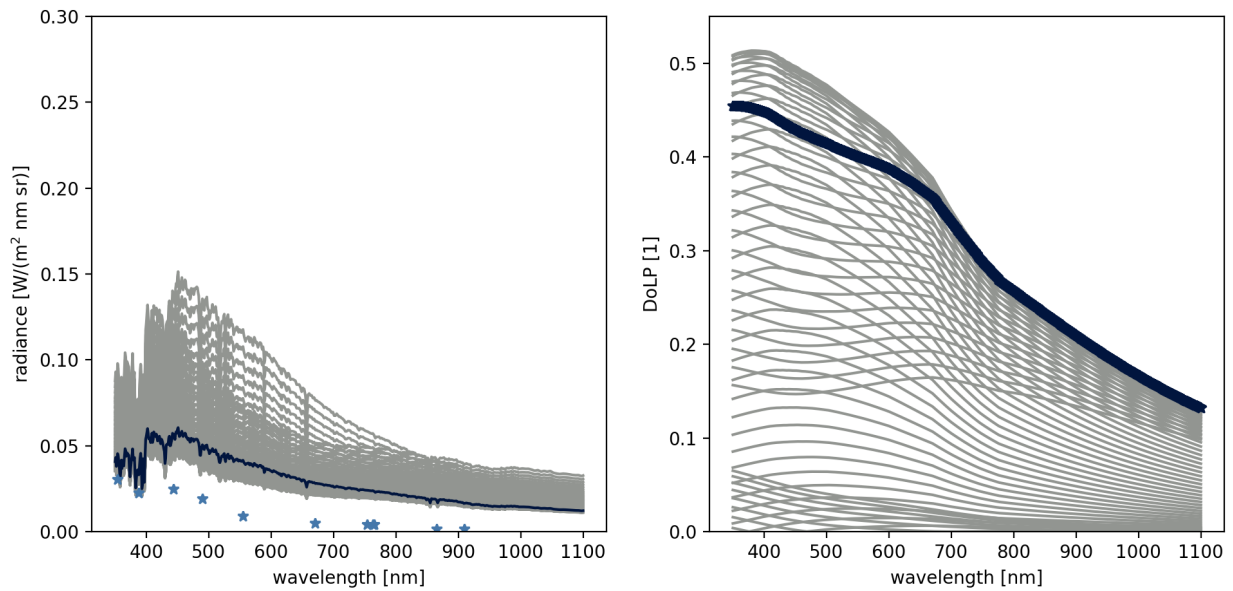
Figure 2 Minimum reference spectrum Lmin for a SZA of 70º and VZA of 30º (black line, left panel: radiance, right panel: degree of linear polarization, DoLP). The grey lines show the ensemble of spectra for -60º <VZA<60º in steps of 2º, the blues asterix indicates correspnding reference values of the 3MI instrument.
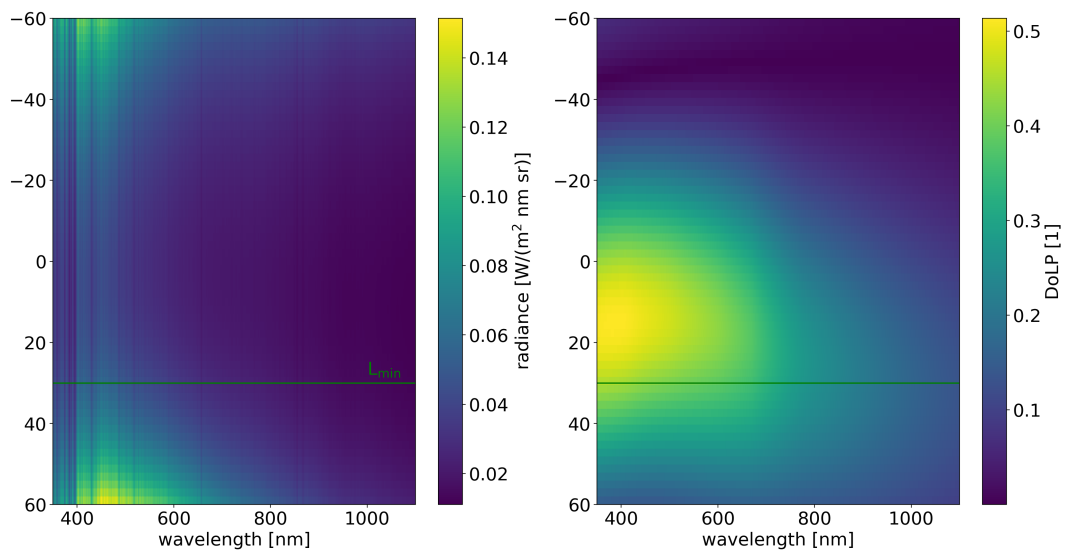
Figure 2 Same as Figure but as a colour contour plot for VZA between -60º and +60º.
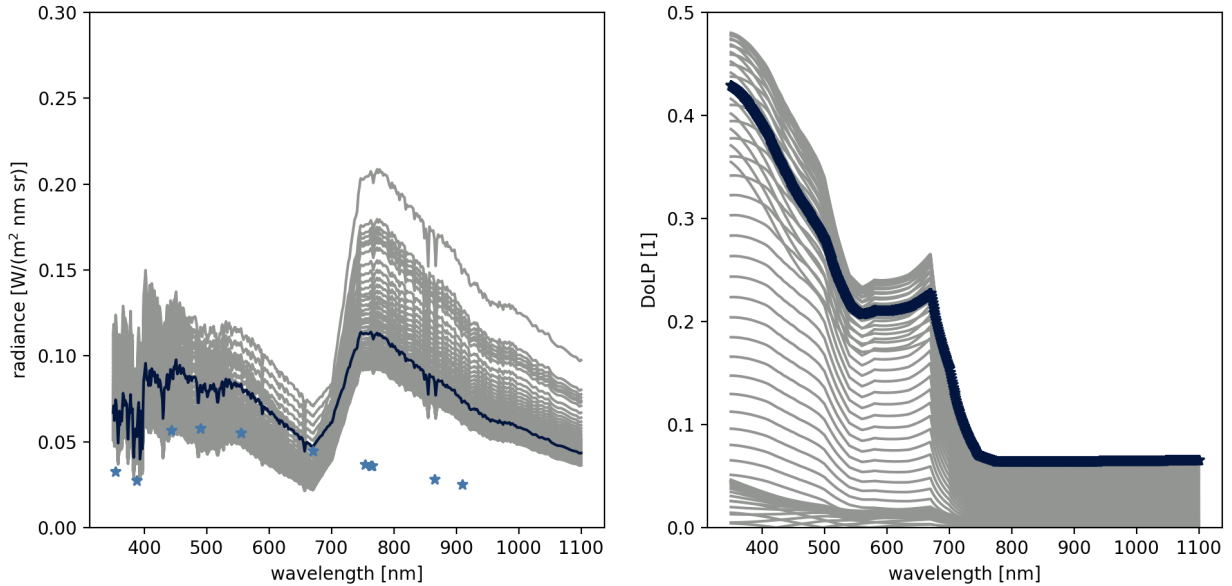
Figure 3 *Same as Fig 2 but for the reference spectra Lref (SZA=50º, VZA = 50º).*
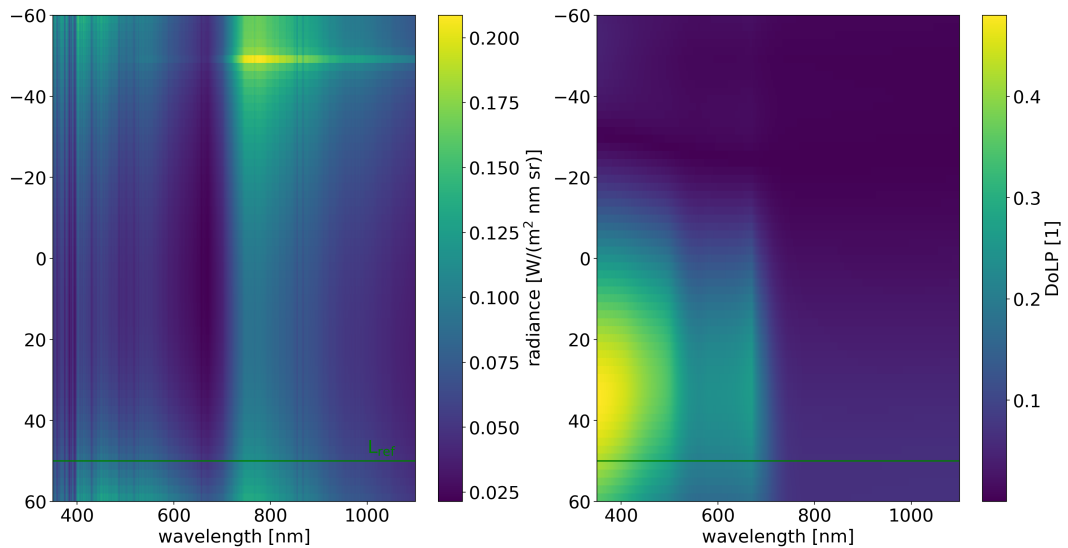
Figure 4 Same as Fig 4 but as a colour contour plot for VZA between -60º and +60º.
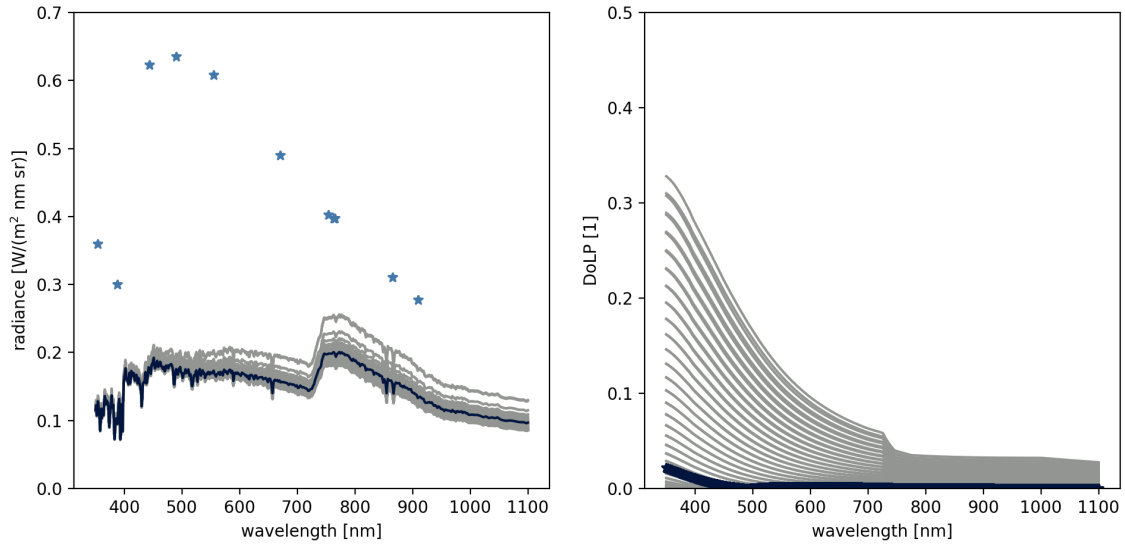
Figure 5 Same as Fig 2 but for the the reference spectrum Lmax (*SZA = 1º, VZA = -20º*).
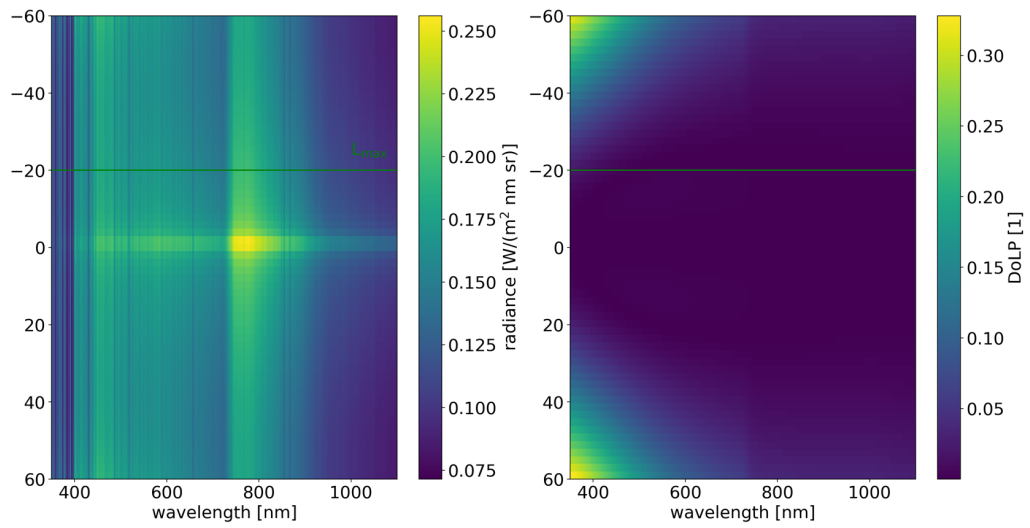
Figure 6 Same as Fig 6 but as a colour contour plot for VZA between -60º and +60º.

Figure 7 Reference spectra Lglint (black) and Lcld_25 (green) and Lcld_50 (blue). For both, Lcld_50 and Lcld_25, the degree of linear polarization is zero due to the assumption of a Lambertian reflector.

4   Potential revision of Lmax

The dynamical range [Lmin, Lmax] is determined to be used as baseline for the MAP performance requirements, assuming global coverage except for desert areas. This choice was made as on expects only a small number of anthropogenic sources at desert areas. This section illustrates a required adaption of Lmax if the bright desert areas should be included as target areas of CO2M. Figure 9 shows the annually mean directional hemispherical reflectance (DHR) for the spectral bands of Polder. Differences to the Lambertian albedo are minor and so we will assume this to be equivalence to the Lambertian

SRON

TECHNICAL NOTE

CO₂M Science

Doc. no.: SRON-CO2M-TN-2018-01
Issue : 1
Date : 6 October 2018
Cat : 4
Page : 9 of 12

albedo in Eq. (1). At the longer wavelength ($\lambda = 865$ nm and $\lambda = 1020$ nm) the desert albedo can reach values of 0.7 in the annual average.
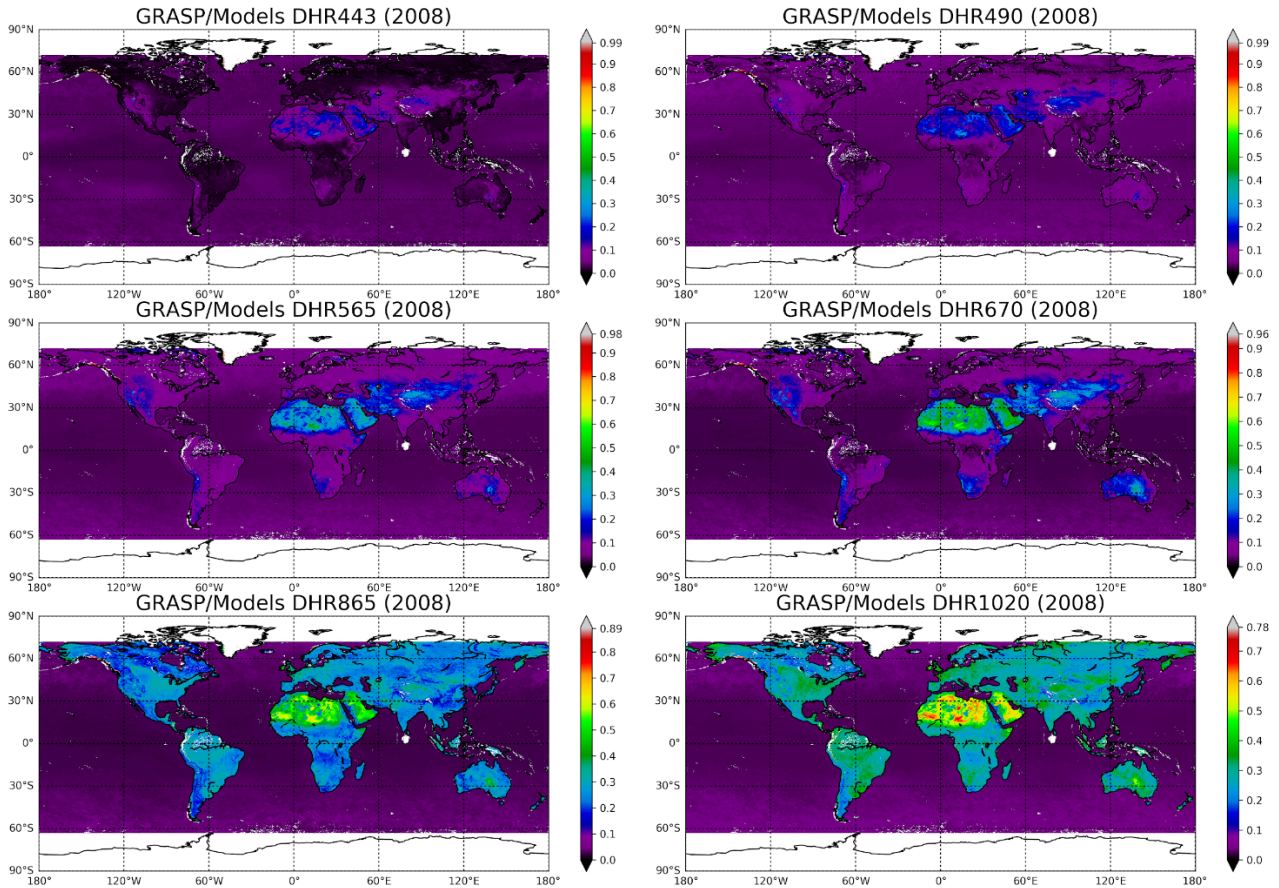
Figure 8: 2018 annual mean directional hemispherical reflectance (DHR) albedo from POLDER data using the GRASP algorithm. The different panels show the albedo for the spectral bands at 443nm, 490nm, 565nm 670nm, 865 nm and 1020 nm. F

Table 2 summarizes the maximum DHR for latitude -60° < θ_{lat} <60° for the different wavelength bands. For our further analysis we select month July (200806) and adjust the spectral albedo value of soil (Guzzi, private communication) with a scaling of 3.7 to match the Polder observations. To be consistent with the Lmax assumptions made for the CO2I spectrometer, we use a maximum threshold of 0.8, which affects only radiance simulations at wavelength λ> 800 nm.

	YYYYMM	MaxDHR443	MaxDHR490	MaxDHR565	MaxDHR670	MaxDHR865	MaxDHR1020
0	200801	0.283036	0.398259	0.514742	0.635518	0.789855	0.794154
1	200802	0.371466	0.423934	0.508754	0.627702	0.766228	0.760870
2	200803	0.286032	0.348347	0.466064	0.595466	0.761720	0.744829
3	200804	0.569447	0.742113	0.731104	0.647688	0.914233	0.888617
4	200805	0.762220	0.886421	0.843239	0.758869	0.786355	0.742237
5	200806	0.254527	0.328650	0.451060	0.604934	0.872039	0.872905
6	200807	0.259753	0.344173	0.451020	0.599307	0.871179	0.842068
7	200808	0.250283	0.340447	0.438166	0.640405	0.792918	0.792354
8	200809	0.266330	0.362565	0.450105	0.619450	0.746521	0.747110
9	200810	0.263156	0.371817	0.458749	0.623284	0.753207	0.755521
10	200811	0.267586	0.370311	0.478233	0.633398	0.749954	0.731438
11	200812	0.273898	0.373323	0.490316	0.654580	0.778721	0.784969

Table 2 Maximum of the monthly averaged DHR for latitude ≤ 60º for the different month of the year 2008.
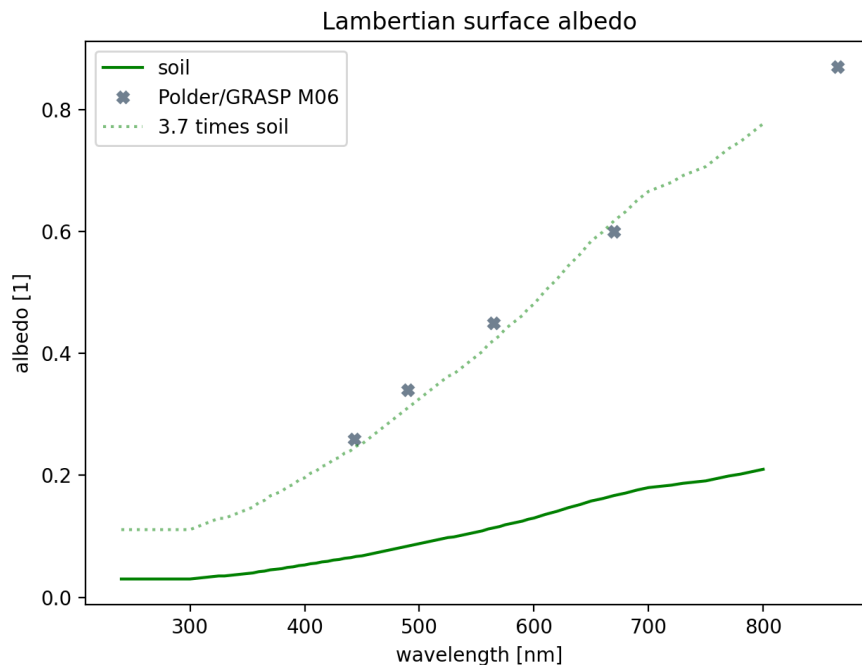
Figure 9 Lambertian surface albedo for soil, monthly averaged DHR from Polder GRASP data for July, 2008 and the soil albedo scaled by a factor 3.7 to fit the GRASP data. Albedo data are from R. Guzzi, private communication.

	TECHNICAL NOTE	**Doc. no.:** SRON-CO2M-TN-2018-01
CO₂M Science		**Issue** : 1
		Date : 6 October 2018
		Cat : 4
		Page : 11 of 12
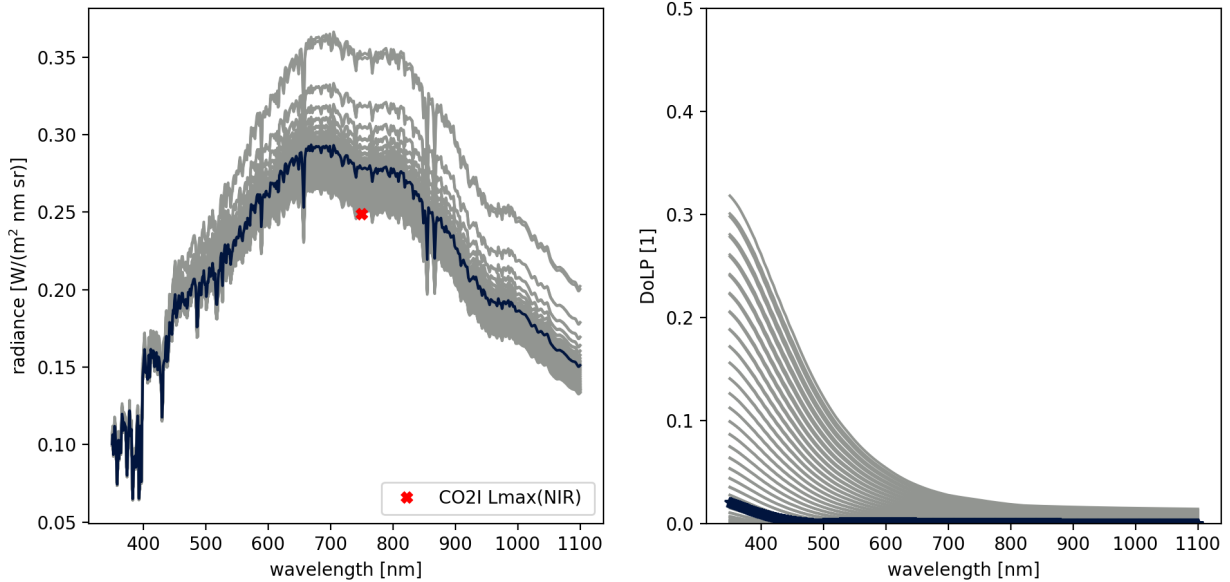
Figure 10 Same as Fig 6 but for a soil surface with scaled surface albedo. The red cross indicates NIR Lmax = 9.4 10^{13} phot/(s cm2 nm sr) of CO2I (MRD V3).
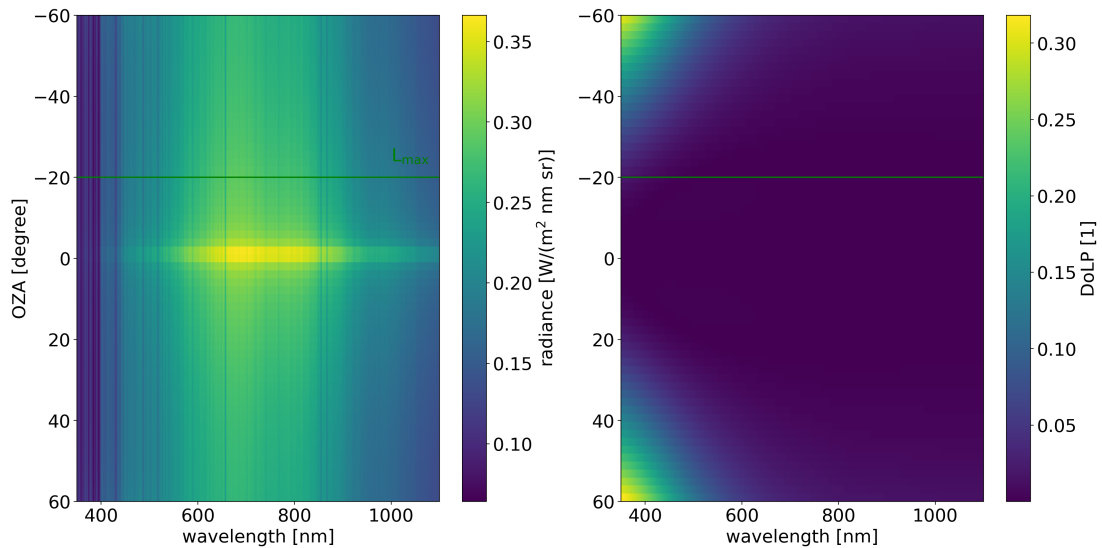
Figure 11 Same as Fig 10 but as a colour contour plot for VZA between -60º and +60º.

Figure 11 and 12 shows the adjusted Lmax radiance and DoLP spectra, where we propose to use a reference spectrum for an observation zenith angle of -20º, which represents a compromise between highest and lowest radiance level of the simulations. Here highest DoLP occurs at shortest wavelengths and is caused by atmospheric Rayleigh scattering and so depends little on the modified surface model. This explains the similarity in DoLP of Fig 6 and 7 on one hand and of Fig. 11 and 12 on the other hand.

S RON

CO₂M Science

TECHNICAL NOTE

Doc. no.: SRON-CO2M-TN-2018-01
Issue   : 1
Date   : 6 October 2018
Cat   : 4
Page   : 12 of 12

5   References

Dubovik, O., Sinyuk, A., Lapyonok, T., Holben, B. N., Mishchenko, M., Yang, P., Eck, T. F., Volten, H., Munoz, O., Veihelmann, B., Zande, v. d. W. J., Leon, J.-F., Sorokin, M., and Slutsker, I.: Application of spheroid models to account for aerosol particle non-sphericity in remote sensing of desert dust, J. Geophys. Res. Atmos., 111, D11208, doi:10.1029/2005JD006619, 2006

A. H. Strahler, J.-P. Muller MODIS BRDF/Albedo Product: Algorithm Theoretical Basis Document Version 5.0, MODIS Product ID: MOD43 Version 5.0 - April 1999

Litvinov P., Hasekamp, O.P., Dubovik O., Cairns, B.:, Model for land surface reflectance treatment: physical derivation, application for bare soil and evaluation on airborne and satellite measurements, J. Quant. Spectrosc. Radiat. Transfer, 113, 2023-2039, doi:10.1016/j.jqsrt.2012.06.027, 2012

Hasekamp, O. P. and Landgraf, J.: A linearized vector radiative transfer model for atmospheric trace gas retrieval, J. Quant. Spectrosc. Ra., 75, 221–238, 2002.

Hasekamp, O. P. and Landgraf, J.: Linearization of vector radiative transfer with respect to aerosol properties and its use in satellite remote sensing, J. Geophys. Res.-Atmos., 110, D04203, doi:10.1029/2004JD005260, 2005a.

P. Schlüssel et al., Post-EPS Mission Requirements Document issue V3c, EUM/PEPS/REQ/06/0043, Eumetsat, 25.June 2010